

The Life Cycle of a Simulated Marine Cyclone: Energetics and PV Diagnostics

G. BALASUBRAMANIAN* AND M. K. YAU

Department of Atmospheric and Oceanic Sciences, McGill University, Montreal, Quebec, Canada

(Manuscript received 4 January 1995, in final form 31 August 1995)

ABSTRACT

The life cycle of an intense marine cyclone is documented in this paper. The departure of the moist dynamics from the dry baroclinic dynamics is explored from an energetics point of view. The contributions of various physical processes through the life cycle to the low-level cyclonic circulation is computed using a recently developed PV (potential vorticity) inversion technique.

The moist cyclone deviates most from the dry cyclone during the early rapid spinup period with significant mesoscale features associated with the warm and bent-back warm frontal zones. However, from an energetics point of view, the moist cyclone possesses a very similar, but enhanced, growth and decay rate during its life cycle. The transports of heat and momentum fluxes are also strengthened. The enhancement of eddy kinetic energy due to condensation accounts for nearly 50% of the maximum eddy kinetic energy generated in the moist cyclone.

From a PV perspective, the main difference between the moist cyclone and the dry cyclone is the production of a low-level PV anomaly during the early rapid spinup period. The cold advection in association with the circulation due to this anomaly has the cyclolytic effect of decreasing the surface thermal anomaly and the cyclogenetic effect of increasing the upper-level wave deepening. In the mature stage when the growth has almost ceased, the dry cyclone also possesses upper- and lower-level PV anomalies very similar to the moist cyclone.

Based on these results, the authors conclude that, except for the mesoscale structural differences and their associated interactions during the early rapid spinup period, the moist cyclone exhibits an enhanced growth rate (and decay rate as well) but appears dynamically similar to the dry cyclone from an energetics point of view as well as in terms of "PV thinking."

1. Introduction

In the past, many studies (Mudrick 1974; Simmons and Hoskins 1978; Takayabu 1986; Polavarapu and Peltier 1990; Thorncroft et al. 1993) have documented the life cycles of dry cyclones. Although they indicated that features simulated in dry, inviscid simulations agree well with the observed synoptic-scale cyclones, it is well known that latent heat release due to condensation can enhance the rapid development of these synoptic-scale systems in a significant manner (Manabe 1956; Danard 1964; Tracton 1973; Gyakum 1983a,b; Liou and Elsberry 1987; Kuo and Reed 1988; Hedley and Yau 1991; Kuo et al. 1991a; Davis and Emanuel 1991). Theoretical linear studies of moist baroclinic waves have represented latent heat release by using a wave-CISK parameterization (e.g., Wang and Barclon

1986; Snyder and Lindzen 1991) or by assuming slantwise neutrality for upward displacements (e.g., Emanuel et al. 1987; Joly and Thorpe 1989). The latter approach was also used by Fantini (1990, 1993) in a two-dimensional nonlinear study of baroclinic instability. A major finding was that the growth rates of the moist wave nearly doubled that of the dry case.

In comparison, only a few published works have focused on the life cycle of moist baroclinic waves in three dimensions. Gall (1976) examined the nonlinear evolution of both dry and moist baroclinic waves in a coarse resolution model ($3^\circ \times 1.8^\circ$) using a moist convective adjustment scheme. The initial zonally constant flow was assumed saturated everywhere. He found that wavenumber 15 dominated in both dry and moist experiments, but the cyclones were much stronger in the moist integration. Gutowski et al. (1992) examined the interaction between moisture and baroclinic eddies through life cycle experiments using a global, primitive equation model. They used 30 waves with initial conditions given by the climatological winter and summer zonally averaged states. A cumulus parameterization scheme and a stable condensation scheme were included. They found that the vertical transports of heat and kinetic energy by the eddies increased by 25%–50% in the moist experiment. Their results based on

* Current affiliation: Program in Atmospheric and Oceanic Sciences/Geophysical Fluid Dynamics Laboratory, Princeton University, Princeton, New Jersey.

Corresponding author address: Dr. M. K. Yau, Department of Atmospheric and Oceanic Sciences, McGill University, 805 Sherbrooke Street West, Montreal, PQ H3A 2K6, Canada.

energetics also indicated that the moist waves exhibited faster evolution of the life cycle. Recently, Whitaker and Davis (1994) examined the dynamics of baroclinic wave growth in a saturated environment employing a parameterization of latent heat release that assumes that all rising air is saturated and the saturated equivalent potential temperature is conserved. They used a domain width of 6000 km and 36 Fourier modes in the meridional direction. Their nonlinear primitive equation simulations show that the growth rate of the moist wave at finite amplitude, associated with the formation of a mesoscale potential vorticity (PV) anomaly generated by latent heat release at the warm front, is significantly faster than the linear growth rate.

While the above three papers have given valuable insight into the development of moist baroclinic wave life cycle, they all employed a relatively crude resolution and a highly simplified condensation scheme. The assumption of a saturated atmosphere precludes the occurrence of convection, both upright and slantwise. Using 30 waves on the globe cannot resolve slantwise convection that has been shown to be the major convective process in the warm frontal regions of winter marine cyclones (Reuter and Yau 1990, 1993). To obtain a quantitative assessment of the effect of convection on the life cycle of marine cyclones, a high-resolution model is called for that can resolve slantwise convection with explicit microphysics. To the authors' knowledge, this has not been done previously.

Recently, Balasubramanian and Yau (1994a, 1994b; hereafter BY94a and BY94b, respectively) explored the physics of convective–cyclogenetic interaction and the quantitative contribution of convection to cyclogenesis during the rapid spinup period. In particular, BY94b addressed the effect of convection on a simulated marine cyclone using a three-dimensional primitive equation model with explicit physics. It was noted that convection leads to intense warm and bent-back warm fronts (Shapiro and Keyser 1990) and it contributes as much as 40% to the deepening of the cyclone. The convection-induced cold advection in the bent-back warm front acts cyclogenetically by strengthening the upper-level vorticity advection but cyclolytically by decreasing the thermal anomaly at the surface.

In BY94a and BY94b, only the departure of the moist cyclone from the dry cyclone during the rapid spinup period was examined and the integration was stopped at 50 h (about 2 days). Therefore, the cumulative effect of convection on the whole baroclinic life cycle and the evolution of the quantitative effect of various physical mechanisms through the life cycle of the simulated marine cyclone were not studied. In this paper, the simulation is carried out on a beta-plane, and the model integration is extended to 240 h (10 days) when the cyclones have decayed. An investigation on the dynamics of the moist and the dry cyclones from an energetics point of view and a PV perspective through their life cycle is carried out.

We emphasize that we have performed a *high-resolution* simulation of a marine moist cyclone life cycle with idealized but realistic initial conditions. Because observations generally show that the atmosphere is predominantly neutral or stable with respect to slantwise convection in winter cyclones, we have been careful to choose an initial state with no convective available potential energy (CAPE) and slantwise convective available energy (SCAPE). This restriction is deemed necessary as experience shows that a rapidly deepening cyclone can be forced quite easily given a large reservoir of convective energy. One of our objectives is to study the effect of convection over the entire life cycle. Another objective is motivated by the results of BY94a and BY94b, which show that the warm and bent-back warm fronts also form in the dry cyclone, with the bent-back appearing at a later time. Thus it is not clear whether convection simply accelerates the cyclogenesis process or whether the dry cyclone would eventually reach the same intensity as the moist run. We will demonstrate that the evolution of energy growth, energy conversions, and the domain-averaged eddy heat and momentum fluxes are qualitatively similar in the dry and the moist cyclones. The amplitude attained, however, is larger in the moist run. Furthermore, though the dry and moist cyclones differ dramatically in the spinup period, they have similar PV anomalies in the upper- and lower-levels in the later stages.

In what follows, we will present a brief description of the evolution of total, eddy, and mean kinetic energies of the simulated moist and dry cyclones until 10 days. The contribution of various physical processes to cyclogenesis through the life cycle is also investigated using the PV diagnostic tool developed by Davis and Emanuel (1991). Organizationally, we will first summarize briefly the model in section 2. The features of the simulated cyclones, energetics, and PV diagnostics are presented in section 3. The concluding remarks are given in section 4.

2. The model

The details of the model are given in BY94b. Originally the model solves the hydrostatic primitive equations on an f -plane. It uses pressure as the vertical coordinate and the Charney–Phillips grid in the vertical. The grid spacing in the horizontal and vertical directions are respectively 25 km and 100 mb. Water vapor and liquid water are treated explicitly. Evaporation of falling water drops is allowed to account for the effects of evaporation-induced downdrafts.

The model domain is a midlatitude channel with vertical walls placed at the north and south boundaries separated by 10 000 km. Periodicity is assumed in the east–west direction. At both the top and bottom boundaries the vertical velocity vanishes. The surface fluxes of heat and moisture are obtained by bulk aerodynamic formulas with a drag coefficient of value $C_D = 1.0$

$\times 10^{-3}$. The model conserves mean zonal momentum only in the absence of momentum fluxes at the boundaries as discussed in Smagorinsky (1956). Therefore, surface momentum fluxes are not included in the formulation.

The major modification here is the inclusion of the linear variation of coriolis parameter in the meridional direction. This beta plane approximation is reasonable for modeling phenomena over a restricted range of latitudes. The values of f_0 and β are $1.0 \times 10^{-4} \text{ s}^{-1}$ and $1.6 \times 10^{-11} \text{ m}^{-1} \text{ s}^{-1}$, respectively.

The basic state is the same as in BY94b obtained by specifying a zonal jet and a sounding at the southern boundary. The zonal jet has a maximum velocity of 35 m s^{-1} at 200 mb and a $1/e$ -folding length of 1200 km. For simplicity we assumed that the initial relative humidity is only a function of height. The temperature and humidity were adjusted by trial and error to produce an initial condition that is potentially neutral to slantwise convection (but conditionally stable) in the center of the domain and stable elsewhere (see Fig. 1c in BY94b). In moist flows, it is well known that conditional stability is more relevant than potential stability.

Added to the basic state is a finite-amplitude geopotential perturbation field (with a corresponding maximum meridional wind speed of 6 m s^{-1} at 500 mb). Since the model atmosphere is unsaturated initially (BY94b), the flow is conditionally stable to slantwise convection with the perturbation. As was shown in BY94b, the model atmosphere becomes potentially unstable with time (up to 25 hours), and the instability is released only when the lower levels are saturated. The sea surface temperature consists of the temperature at 1000 mb and a Gaussian perturbation of magnitude 15 K and a $1/e$ -folding length of 500 km. The sea surface temperature is held constant during the integration. We have used a higher value of 15 K for the SST anomaly to obtain enhanced surface heat and moisture fluxes before the rapid spinup. Such high values of SST anomalies have been observed during the winter (Hedley and Yau 1991).

As in Thorncroft et al. (1993), we found that the life cycle of the *dry cyclone* was independent of the initial perturbation. If the amplitude of the perturbation was larger, the life cycle was identical except for the timing. However, the maximum deepening of the *moist cyclone* depends on the location of the maximum SST in relation to the initial cyclone center. For the results presented in this paper, we adjusted the position of the initial cyclone center such that the cyclone passes over the maximum SST during the rapid spinup period. The warming of the boundary layer before the passage of the storm has a larger impact (Kuo et al. 1991b) than after passage. The sensitivity of the moist cyclone to the position and amplitude of the SST anomaly has been discussed in Balasubramanian and Yau (1995).

3. Results

a. Some features of the simulated moist and dry cyclones

Figure 1 shows sharp deepening of the surface system for both cyclones until day 4. Thereafter, the systems fill quite rapidly, suggesting rapid barotropic decay. Weak redevelopment occurs after day 6 (see also broad secondary peaks in eddy kinetic energy in Fig. 4), consistent with results in two-dimensional baroclinic wave equilibration studies by Nakamura and Held (1989) and three-dimensional f -plane simulations by Polavarapu and Peltier (1990).

On day 4, at the time of maximum intensity, the moist cyclone departs from the dry one by as much as 25 mb. In terms of pressure drop, latent heating from condensation contributed more than 25% to overall cyclone development.

BY94b presented the mesoscale structures of the f -plane moist cyclone at 25 and 45 hours and provided evidence for slantwise convective adjustments in the warm and bent-back warm frontal regions consistent with observations (Bennetts and Sharp 1982; Sanders and Bosart 1985; Emanuel 1988; Reuter and Yau 1990, 1993). Here we present results on day 4 (96 hours) and illustrate the evolution of the upper level Ertel's potential vorticity.

The moist cyclone (Fig. 2a) is deeper than the dry cyclone (not shown) by about 25 mb. The gradients are much stronger in the moist case (see the crowding of the isobars along the bent-back warm front that extends to the south of the cyclone center). The cyclones tilt in the northwest-southeast orientation and resemble the cyclonic type (LC2) depicted in Thorncroft et al. (1993).

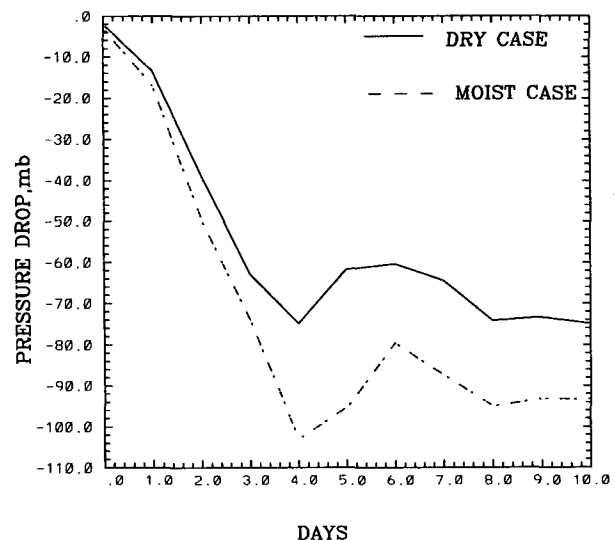


FIG. 1. Evolution of surface pressure deviation in mb for the moist and dry runs.

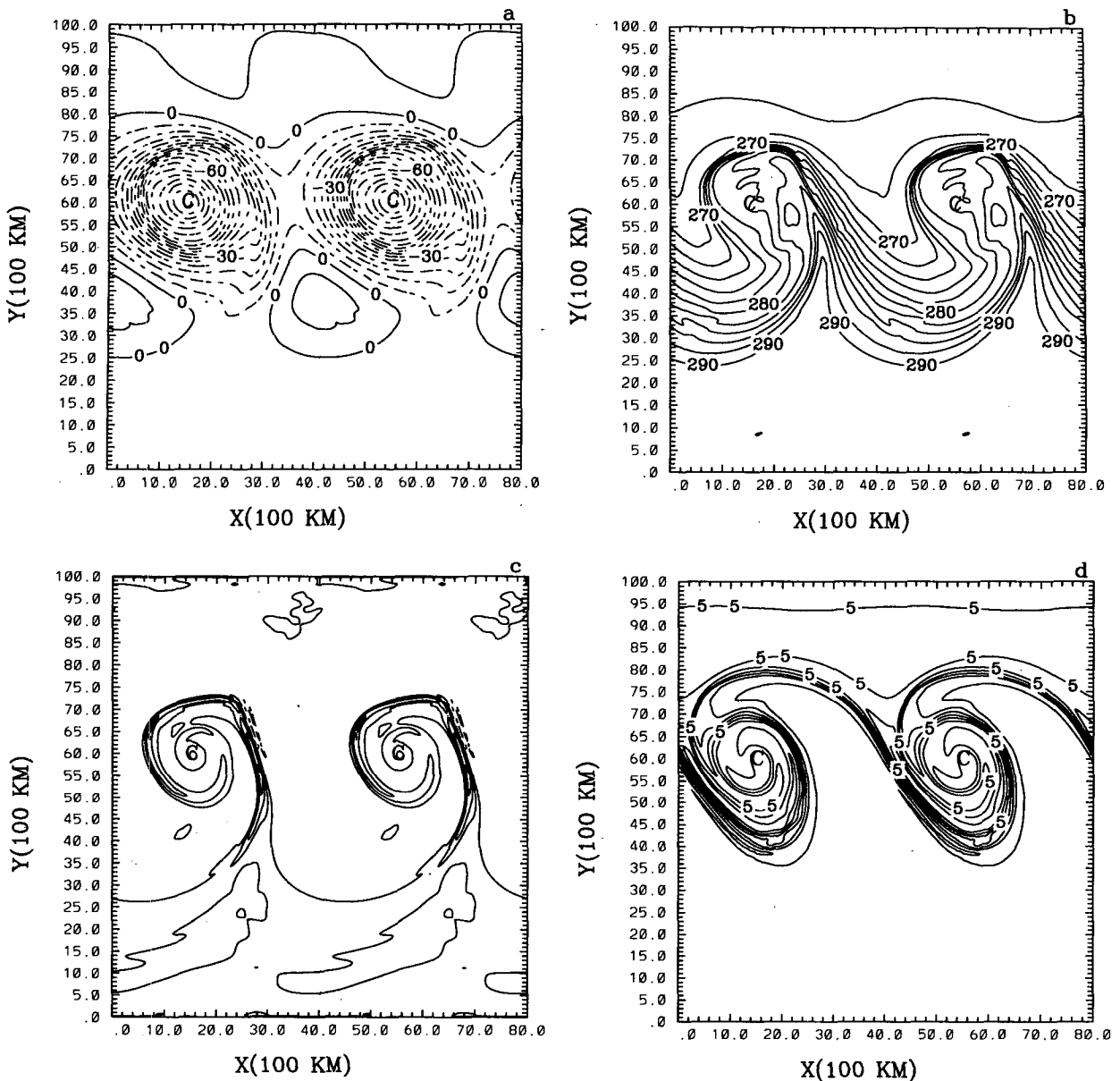


FIG. 2. The features of the moist cyclone on day 4. (a) The surface pressure deviation every 6 mb, (b) temperature at 900 mb every 2 K, (c) vorticity at 950 mb every $1.0 f_0$, and (d) Ertel's potential vorticity at 300 mb every 1.0 pvu. The label "C" represents center of surface cyclone.

The warm front formed earlier than the cold front in agreement with the PE simulations of Rotunno et al. (1994). The warm front on day 4 is located more than 1000 km north-northeast of the cyclone centers (Fig. 2b). In the moist run, the thermal gradient in the bent-back warm frontal region is extremely intense and the bent-back warm front extends to the south of the cyclone center. In the dry cyclone (not shown) both the cold and warm fronts have comparable thermal gradients. However, the warm front in the moist cyclone is

much stronger than the cold front, contrary to results from dry simulation of baroclinic waves (Polavarapu and Peltier 1990). A similar result was obtained by Joly and Thorpe (1989) in their study of baroclinic waves with a parameterization for slantwise convection. The baroclinicity becomes weak near the center of the domain. Intense baroclinic zones are being displaced to the south and north as in previous life cycle studies (Simmons and Hoskins 1978; Polavarapu and Peltier 1990).

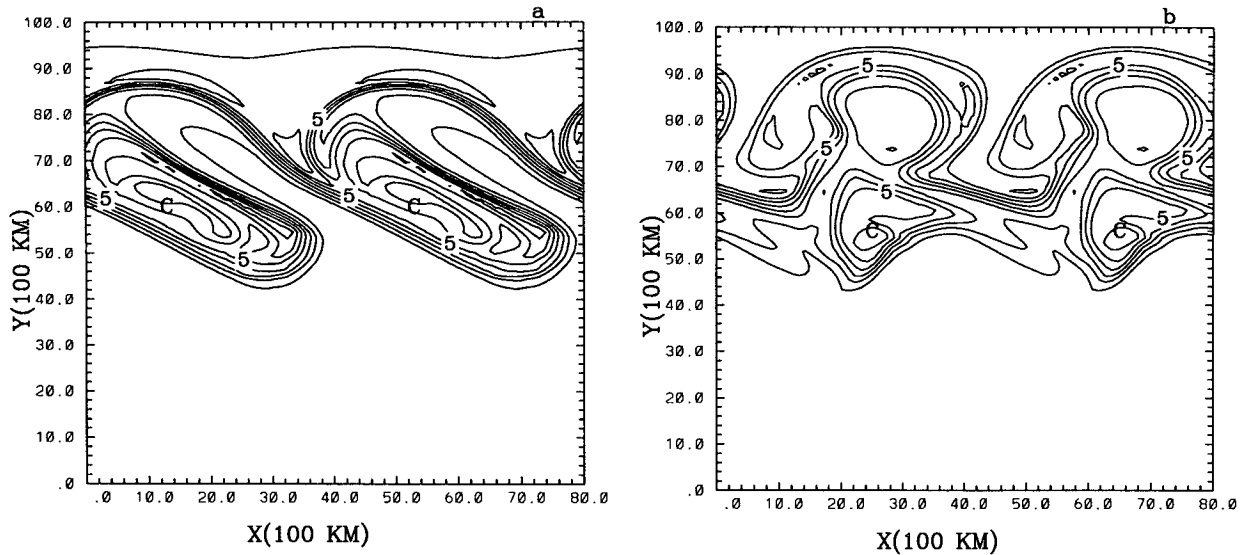


FIG. 3. Ertel's potential vorticity on $\theta = 320$ K surface for the moist cyclone on (a) day 5 and (b) day 7. The contour interval is 1.0 p.u.v.

The vertical components of the relative vorticity (ζ) at 950 mb in the dry (not shown) and the moist (Fig. 2c) cyclones are concentrated along the regions of the warm front and the bent-back warm front. The cyclone centers, however, exhibit almost vanishing circulation. The maximum values on day 4 in the two cases are 4.8 and $4.2f_0$, respectively. We noticed that the vorticity reached maximum values of $10.8f_0$ on day 2 in the moist case and $7.4f_0$ on day 5 in the dry case. The vorticity in both cyclones shows a very narrow horizontal scale of 200 km. The regions with dashed contours in Fig. 2c suggest that locally the flow is weakly stable to inertial instability as the absolute vorticity ($f_0 + \beta y + \zeta$) becomes vanishingly small.

The enhanced upper-level wave development in the moist cyclone can be inferred from a comparison of Ertel's PV at 300 mb. We plotted the PV on a pressure surface here to infer the effect of vertical transports at the upper levels. Because PV is a conserved quantity on upper-level potential temperature (θ) surfaces, the PV contours plotted on θ surfaces would simply be advected around and further analysis is needed to determine the vertical transports. In the moist cyclone (Fig. 2d), the PV contours extend more to the south and its maximum value (>8.0 p.u.v.) exceeds that of the dry case (not shown). Since the upper-level wave development is stronger in the moist cyclone and the stratosphere is a reservoir of high PV values, much more air of stratospheric origin must have descended down through the 300-mb surface in the case of the moist cyclone. The striking similarity of these contours to those presented for LC2 in Thorncroft et al. (1993) indicates that the systems studied in this paper are predominantly cyclonic.

To check if our model conserves PV on isentropic surfaces, we also computed the PV field on days 5 and 7 on the $\theta = 320$ K surface. The results are obtained by interpolating the PV values from the pressure surfaces to the θ surfaces. The maximum values of PV on day 5 are 7.6 p.u.v. for the moist cyclone (Fig. 3a) and 7.3 p.u.v. for the dry cyclone (not shown), illustrating the conservation of PV on the $\theta = 320$ K surface, which is located near the tropopause in the middle of the channel. The moist case shows stronger wave development as indicated by the stronger gradients of PV. The slightly more southward extension of the contours in the moist case noted above persists through day 5 (Figs. 3a). Note that the PV pattern indicates a northwest-southeast orientation because the evolution of PV occurs mainly on the cyclonic side of the shear. The barotropic decay process results in an increase in the zonal extent of the PV field. By day 7, a complete Rossby wave breaking event (Edmon et al. 1980) has taken place (Fig. 3b).

b. Energetics

The eddy (departure from zonal mean) kinetic energy (KE) peaks on day 4 for both cases (Fig. 4). The mean KE starts to rise steeply at the same time as found by Simmons and Hoskins (1978, 1980). The trend of the total KE is quite similar to that of the eddy KE until the latter reaches its peak. During the eddy growth period, there is little change in mean KE, suggesting that the eddies grow at the expense of the available potential energy (APE). After day 4, the total KE does not show much growth, while there is an immense amount of energy exchange between mean and eddy KE. At the

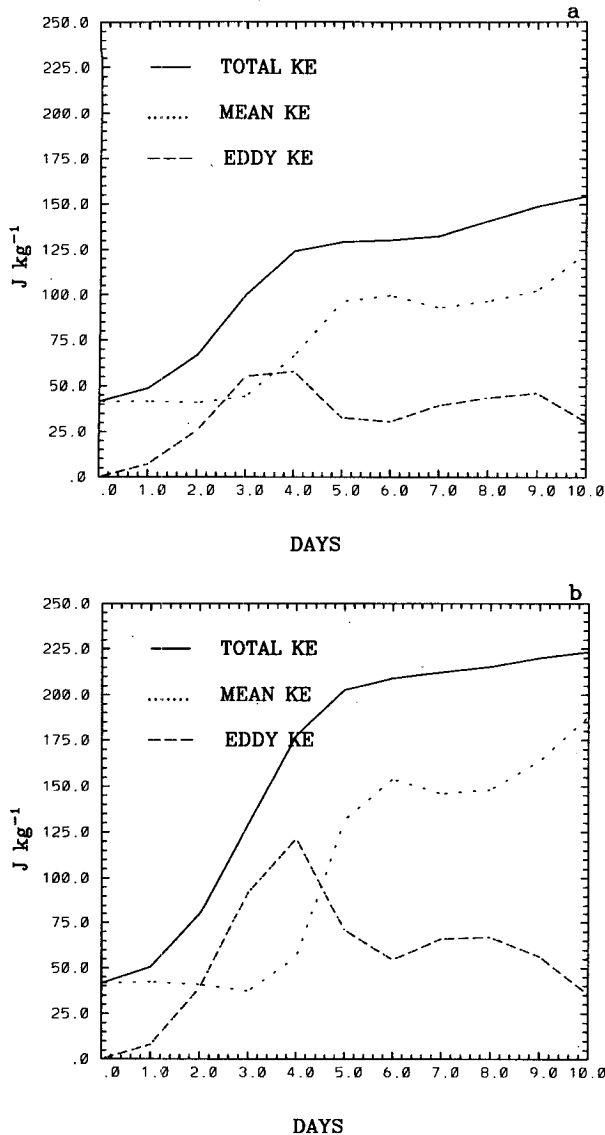


FIG. 4. Evolution of total, zonal (mean) and eddy kinetic energy in (a) dry cyclogenesis and in (b) moist cyclogenesis.

end of the simulation, the baroclinic wave growth has resulted in the acceleration of the mean flow with latent heat release acting to enhance the acceleration. In terms of the peak eddy KE achieved, latent heat release contributes about 50% to the overall eddy energy growth (120 J kg^{-1} in the moist case and 60 J kg^{-1} in the dry case).

We calculated the different conversion terms in the eddy KE following Lorenz (1955). The eddy KE tendency equation is

$$\frac{\partial K_E}{\partial t} = C_E + C_K - D_E, \quad (1)$$

where

$$K_E = \frac{1}{2} \int_0^{P_0} \overline{u^{*2} + v^{*2}} dp \quad (2)$$

$$C_E = -R \int_0^{P_0} \overline{T^* \omega^*} dp/p \quad (3)$$

$$C_K = - \int_0^{P_0} \left(\overline{[u^* v^*] \frac{\partial}{\partial y} + [u^* \omega^*] \frac{\partial}{\partial p}} \right) [u] dp - \int_0^{P_0} \left(\overline{[v^* \omega^*] \frac{\partial}{\partial y} + [v^* \omega^*] \frac{\partial}{\partial p}} \right) [v] dp \quad (4)$$

$$D_E = - \int_0^{P_0} \overline{u^* F_x^* + v^* F_y^*} dp. \quad (5)$$

In the above expressions, square brackets denote a zonal mean, an overbar indicates an average over a pressure surface, and * denotes the departure from zonal mean. The term C_E in (3) is the energy conversion from eddy APE to eddy KE. A positive correlation between eddy vertical motion and eddy temperature ($[\omega^* T^*] < 0$) results in conversion of eddy APE to eddy KE. We noticed that the first term in the expression for C_K in (4) was an order of magnitude larger than the other three terms. This term ($-[u]_y [u^* v^*]$) represents the barotropic decay in our model. The eddies give up their energy to the mean flow and decay if they tilt with the horizontally sheared mean flow ($-[u]_y [u^* v^*] > 0$). The diffusion term in (5) was found to be very small.

The evolution of the rate of energy conversion, from eddy APE to eddy KE (C_E) and from zonal KE to eddy KE (C_K), is similar for both cyclones (Fig. 5), though the moist case exhibits larger rates. Note that the timings of the peaks of eddy APE to eddy KE conversion for the two cyclones are the same. The conversion from zonal KE to eddy KE peaks on day 5 for the moist cyclone and on day 4 for the dry cyclone. From an energetics point of view, one can conclude from Figs. 4 and 5 that the moist cyclone exhibits baroclinic dynamics that is similar to but greater than the dry cyclone during both development and barotropic decay. This view is further supported by the behavior of other quantities such as horizontal eddy heat and momentum fluxes.

The meridional cross sections of eddy KE density indicate two local maxima at 300 and 1000 mb (Figs. 6a and 6b). This double maximum is similar to the vertical distribution of eddy KE for wavenumber 8 (wavelength at $45^\circ = 3536 \text{ km}$) in the dry experiment by Gall (1976).

In the case of the moist cyclone, there was a concentration of eddy KE on day 2 near the warm front (figure not shown), consistent with the finding of BY94b that the release of latent heat near the warm frontal zone leads to an asymmetry in the development of the wave. Xu (1988, 1990) also found that a zone

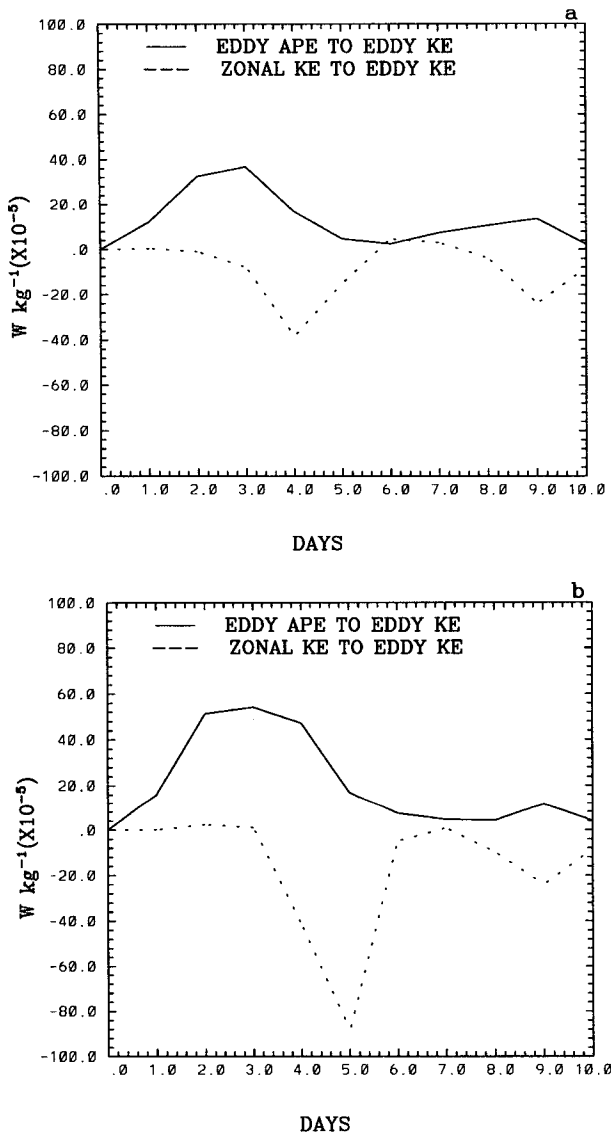


FIG. 5. Evolution of the energy conversion between eddy available potential energy and eddy kinetic energy and between zonal mean kinetic energy and eddy kinetic energy in both (a) dry and (b) moist cyclogenesis.

of small moist symmetric stability embedded in a baroclinic basic state can trap energy when the wave develops. In comparison to the dry run (Fig. 6a), the moist run (Fig. 6b) shows a much stronger eddy development in the upper levels (maximum values of 350 and $700 \text{ m}^2 \text{ s}^{-2}$). The mechanism for the enhanced upper-level growth is discussed in BY94a and BY94b, where we showed that the stronger cold advection associated with the bent-back warm front leads to further intensification of the upper-level wave in the moist cyclone.

The horizontal eddy momentum fluxes ($[u^*v^*]$) play an important role in the decay of the eddies (James

1987; Nakamura 1993). The meridional cross section (Fig. 7) of the momentum fluxes on day 4, when the conversion from eddy to zonal KE is near its maximum (Fig. 5), depicts a double maximum in both cyclones, with one located near the surface and the other near the level of the tropopause. It should be noted that the fluxes are directed predominantly to the south; a feature also found in the normal modes of Cartesian f -plane PE models in previous studies (Snyder et al. 1991; Nakamura 1993; Rotunno et al. 1994). However, observational studies (Paused and Oort 1984) and the experiments on the sphere with a wavenumber 6 disturbance (Simmons and Hoskins 1978, 1980) have exhibited predominantly poleward fluxes. We shall address the implications of the sign of the momentum fluxes to wave equilibration and the type of wave breaking in spherical and Cartesian geometries in a future paper.

From Figs. 4 and 5, it appears that the eddies grow as well as decay faster when the latent heat release is included. The faster decay (which depends mostly on $-[u]_y[u^*v^*]$) in the moist case (Fig. 5) is related to the enhancement of the eddy momentum fluxes (Fig. 7b) during the wave growth and the feedback between the mean flow and the momentum fluxes (James 1978; Nakamura 1993). The overall increase of the equatorward momentum fluxes in the moist cyclone is also illustrated in Fig. 8b.

The meridional cross sections of horizontal eddy heat transport ($[v^*T^*]$) for the dry and moist cyclones (not shown) showed that in both cases, the northward heat fluxes remained largely confined to the lower troposphere. On the 900-mb surface, the horizontal eddy heat flux (v^*T^*) in the moist cyclone (not shown) is larger on day 4 when its eddy KE reaches a maximum.

The domain-averaged horizontal eddy heat and eddy momentum fluxes (Fig. 8) shows similar behavior for the two cyclones, except that the amplitude is much larger in the moist case. While the heat fluxes attain their maxima during the baroclinic growth (around day 3), the momentum fluxes do so during the barotropic decay period (day 4–5). In summary, the distributions of EKE, eddy heat, and momentum fluxes indicate that the moist cyclone possessed a similar, but enhanced, growth rate and transport of heat and momentum fluxes.

c. PV diagnostics

The PV inversion technique developed by Davis and Emanuel (1991) and used in BY94b is adopted to quantify the contribution of various physical processes to the life cycle of the storm. In our hydrostatic pressure coordinate model the potential vorticity P (which is conserved in a Lagrangian sense in the absence of diffusion and diabatic sources) is given by

$$P = -g \left[\left(f + \frac{\partial v}{\partial x} - \frac{\partial u}{\partial y} \right) \frac{\partial \theta}{\partial p} - \frac{\partial u}{\partial p} \frac{\partial \theta}{\partial y} + \frac{\partial v}{\partial p} \frac{\partial \theta}{\partial x} \right]. \quad (6)$$

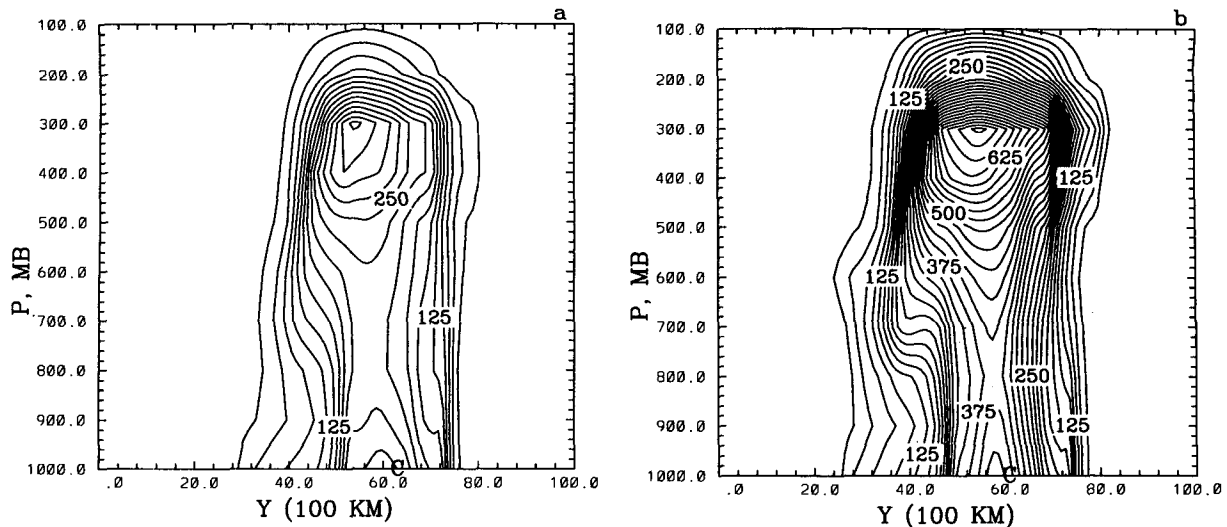


FIG. 6. (a) The meridional cross section of zonally averaged eddy kinetic energy on day 4 for the dry cyclone. The same cross section for the moist cyclone is shown in (b). The contour interval is $25 \text{ m}^2 \text{ s}^{-2}$.

The mean PV, geopotential, and streamfunction are calculated from the initial basic state. The surface (1000 mb) θ anomaly (θ_B), the low-level (900 to 600 mb), and the upper-level (500 to 100 mb) PV anomalies (LPV and UPV) are calculated daily. The individual flow associated with each anomaly is obtained by inversion using a horizontal grid length of 100 km.

Compared to the dry case, there is a dramatic departure of the θ_B at the center of the moist cyclone (location of minimum ϕ' at 1000 mb obtained from ϕ' at 950 and 850 mb) on days 1–3 (Fig. 9a). This behavior is caused by the encroachment of cold advection into the cyclone center when the bent-back warm front forms rapidly. Although

the temperature anomaly also decreases in the dry cyclone after day 2, the rate of decrease is much more gradual.

For the moist cyclone (Fig. 9b), latent heat release in the warm front caused a sudden increase of positive LPV starting on day 1. It reaches a peak value of 1.5 pvu ($\text{pvu} = 10^{-6} \text{ m}^2 \text{ K kg}^{-1} \text{ s}^{-1}$) on day 3 (averaged over a $100 \text{ km} \times 100 \text{ km}$ area but exceeds 3.7 pvu in the bent-back warm frontal region when calculated on the $25 \text{ km} \times 25 \text{ km}$ grid mesh). The evaporation of falling water would normally counteract the increase of LPV. This is not the case because the warm frontal region where condensation occurs is saturated. For the dry cyclone, the maximum PV anomaly at 800 mb also

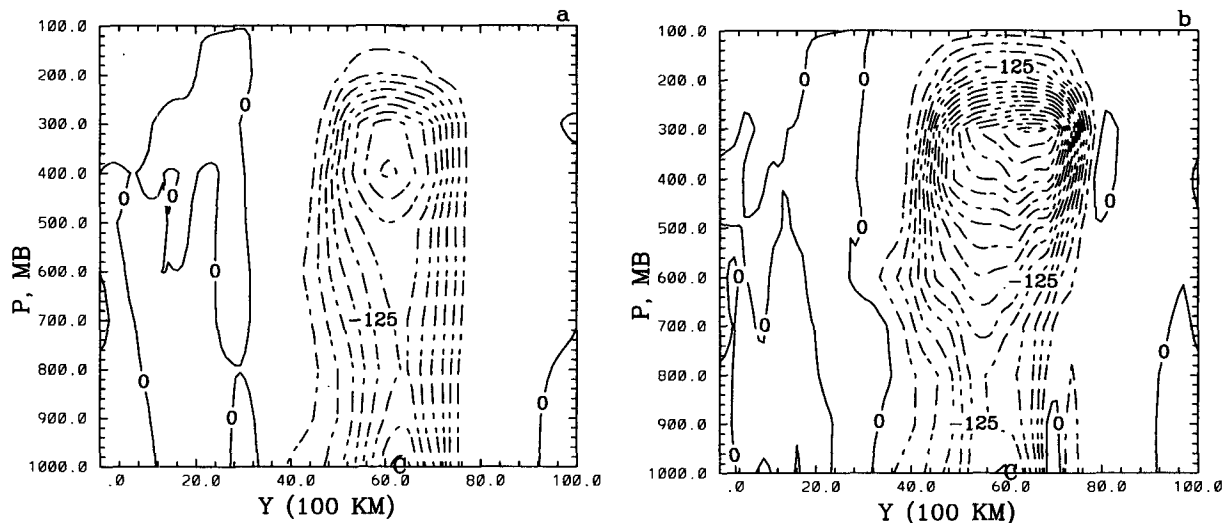


FIG. 7. The meridional cross section of zonally averaged eddy momentum fluxes on day 4 for (a) the dry cyclone and (b) for the moist cyclone.

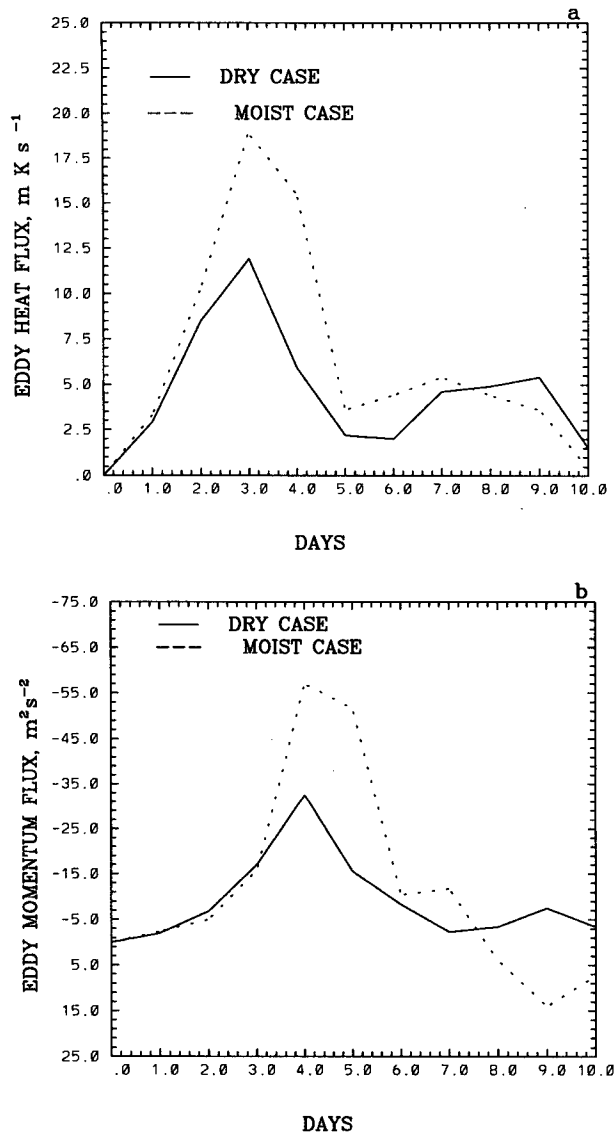


FIG. 8. The evolution of the domain averaged (a) eddy heat fluxes and (b) eddy momentum fluxes for the dry and moist cyclones.

shows a significant rise throughout the whole life cycle and has a magnitude similar to the moist case during the decay stage. Later it is shown that diffusive effects in the model can produce LPV comparable to that produced by condensation. Note that the 800-mb production of negative PV anomaly is much weaker and, as will be shown later, is located to the southeast far away from the cyclone center. Its influence on cyclogenesis is therefore expected to be small.

The evolution of the maximum PV anomaly over the cyclone center at 300 mb (Fig. 9c) shows larger positive values for the moist case. The difference between the runs reaches 2.2 pvu on day 2. BY94b showed that the trough center advances much closer to the cyclone

center during the rapid deepening period and the upper-level trough deepens rapidly from the sudden onset of cold advection below. The enhanced influence of upper-level wave on the surface moist cyclone is borne out by the location of maximum PV at 300 mb directly over the cyclone center.

Since positive PV is not produced by condensation in the upper troposphere, air of stratospheric origin must have descended due to an intensified secondary circulation (sinking motion behind the cyclone). Because upper-level frontogenesis is also augmented (see Fig. 2d), a feedback between sinking motion and the Q -vector geostrophic forcing, called "Shapiro effect" (Rotunno et al. 1994), can be operating at the upper level. Note negative PV values are slightly larger in the moist case because condensation produces positive (negative) PV anomalies below (above) the level of maximum upward motion (Eliassen and Kleinschmidt 1957).

The minimum PV associated with the ridge at 300 mb (Fig. 9c) is stronger also in the moist case. This ridge intensification results from the transport of negative PV, produced above the level of maximum condensation, by the warm conveyor belt (Eliassen and Kleinschmidt 1957). The intensified ridge, together with the deepening upper-level trough, no doubt contributes to the enhanced vorticity advection in the moist cyclone. The enhancement of negative PV anomaly due to condensation in the upper levels (Fig. 9c) is not as dramatic as the increase in the low-level positive PV anomaly (Fig. 9b). This is due to the fact that the decrease in PV in the upper levels due to condensation must exactly balance the increase in PV in the lower levels as a mass-weighted integral (Thorpe and Emanuel 1985). While the positive anomaly in the lower levels indicates a meso-scale structure, in the upper levels the negative anomaly is distributed over a large-scale ridge (see Figs. 13b and 13c in BY94b).

The total 900-mb geopotential deviation from the initial mean state and the contribution to this deviation from the anomalies θ_B , LPV, and UPV are plotted in Fig. 10. The percentage contribution of these three dynamically significant anomalies to the 900-mb geopotential deviation is listed in Table 1. The deviation values are calculated at the cyclone center. The geopotential deviations associated with θ_B (Fig. 10b) are quite different for the two cases during the period 1–3 days. The cold advection in the bent-back warm frontal region of the moist cyclone, which is intense at this time (see the quasi-Lagrangian thermal advection plotted in Fig. 18 of BY94b) decreases the geopotential anomaly associated with θ_B until day 3 relative to the dry case. Table 1 shows that on day 3, θ_B contributes as low as 12.8% to moist cyclogenesis while it accounts for 40.5% of the dry cyclogenesis. In the final stages of the storm (after day 5) the

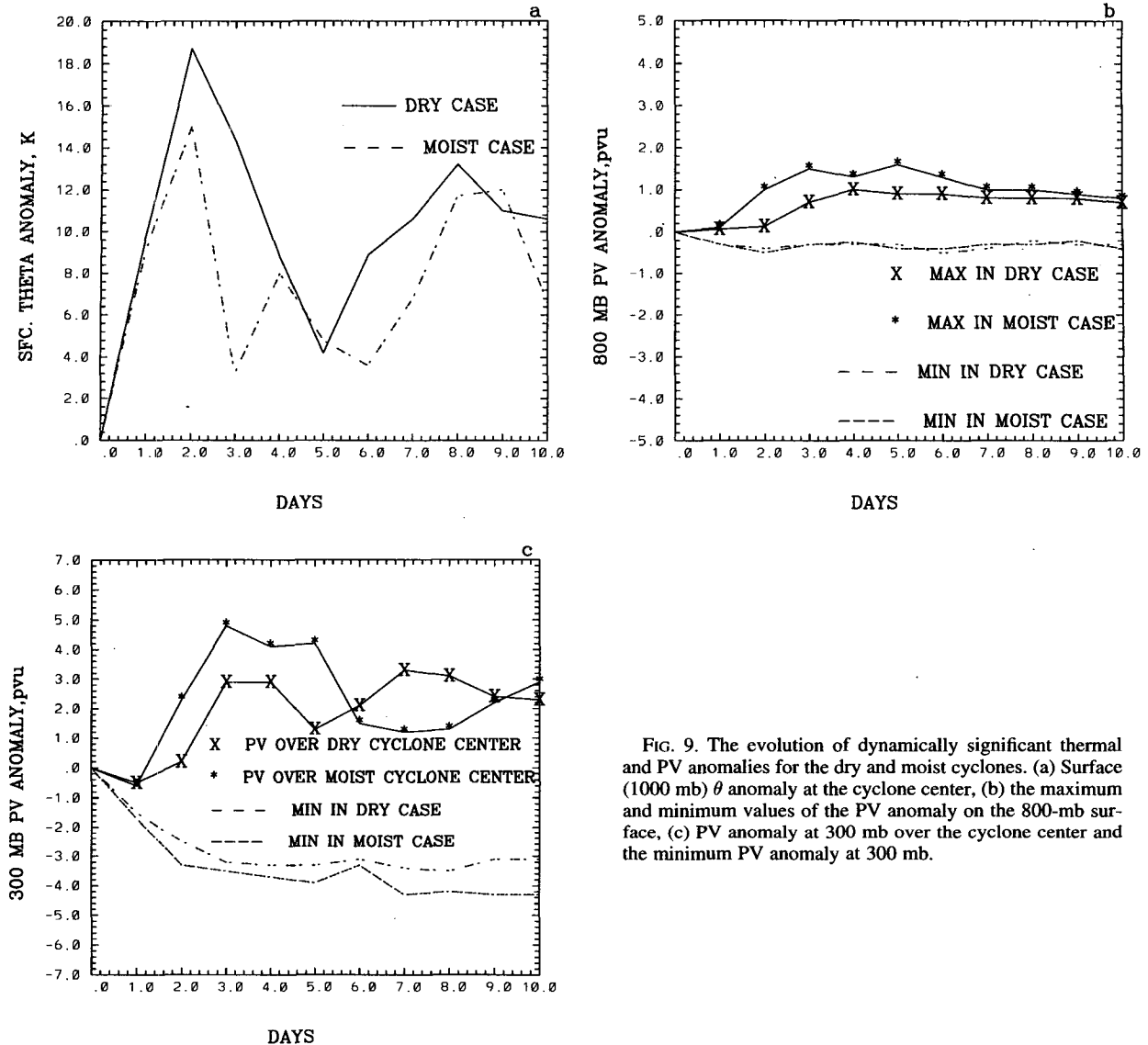


FIG. 9. The evolution of dynamically significant thermal and PV anomalies for the dry and moist cyclones. (a) Surface (1000 mb) θ anomaly at the cyclone center, (b) the maximum and minimum values of the PV anomaly on the 800-mb surface, (c) PV anomaly at 300 mb over the cyclone center and the minimum PV anomaly at 300 mb.

θ_B contributes about 30%–35% to the storm depth in the dry and the moist cyclones.

The 900-mb geopotential deviations associated with LPV (Fig. 10c and Table 1) indicate significant difference between the runs on day 3. This difference is as high as 17 dam. However, the percentage contribution of LPV to dry cyclogenesis also increases in association with the appearance of LPV in the bent-back warm frontal region. After day 4, the circulation associated with the LPV constitutes 20%–30% of the 900-mb geopotential deviation in both cases. Therefore, the moist and dry cyclones appear dynamically similar also in terms of “PV thinking,” except for the appearance of a mesoscale LPV in the moist case during the early stage of spinup.

The impact of the UPV on cyclogenesis (Fig. 10d) in the moist cyclone shows increased contribution. The

contribution of UPV is much larger in the moist cyclone between days 2 and 5. This behavior is consistent with the findings of BY94a and BY94b that the convection-induced cold advection in the bent-back warm frontal region leads to stronger development of the upper-level wave. The intensification of the upper-level wave is related to the enhanced differential thickness advection in the tendency equation of the quasigeostrophic theory (Holton 1992). Although the geopotential deviation associated with UPV is larger in the moist case, the percentage contribution of UPV (Table 1) in both the moist and dry cyclones is about the same (about 40%) in the final stages of the storm.

The fields of θ_B , PV anomaly at 800 and 300 mb, as well as their associated nondivergent winds at 900 mb on day 5, are plotted in Fig. 11 for the dry and moist runs. In the PV inversion procedure, the

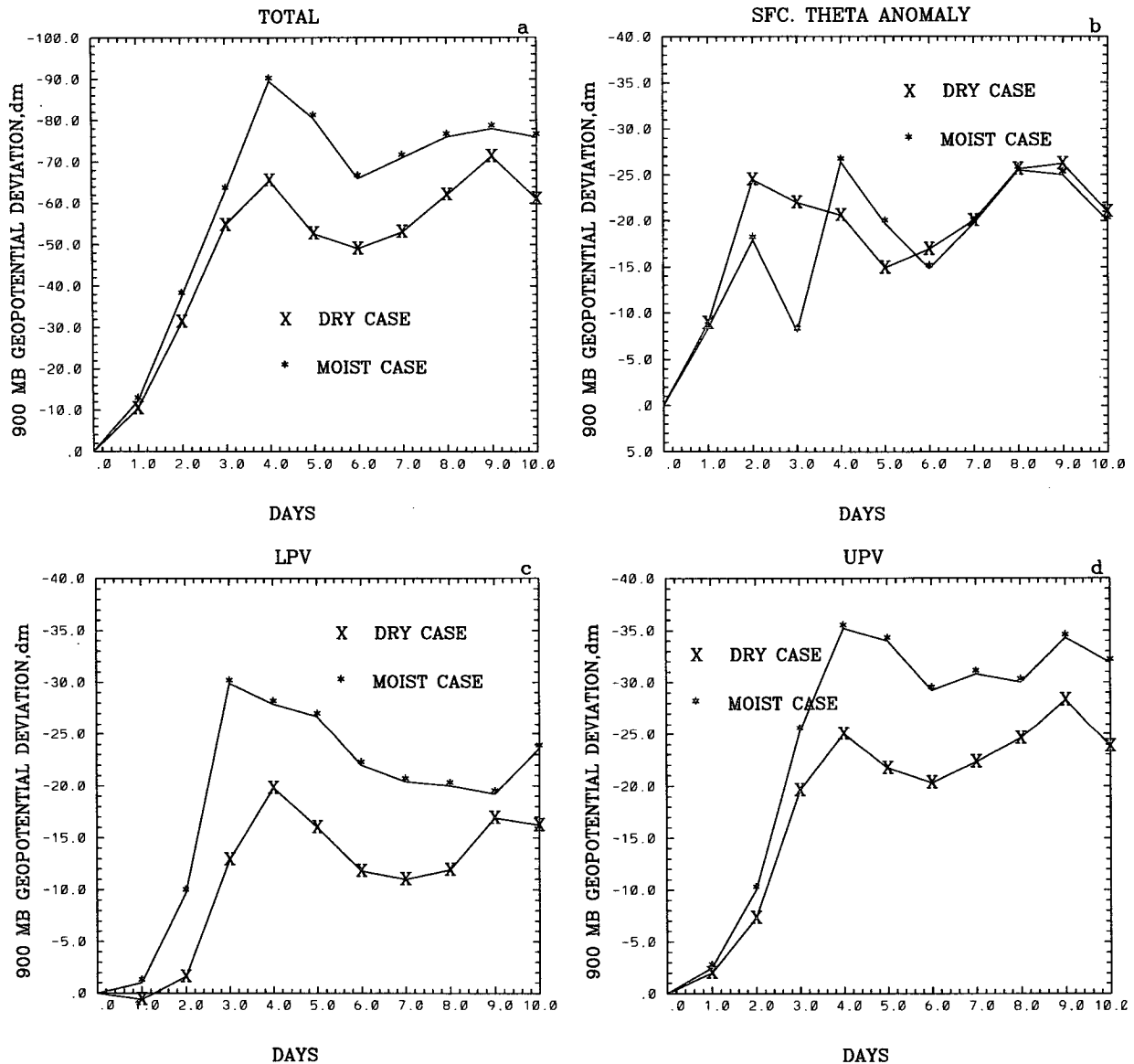


FIG. 10. The results of PV diagnostics for the dry and moist cyclones. The evolution of (a) total geopotential deviation at 900 mb over the cyclone center, the contribution of (b) surface θ anomaly, (c) LPV anomaly, and (d) UPV anomaly to the total anomaly in (a). (In the ordinates, dm denotes decameters.)

assumption has been made that the rotational winds are much greater than the divergent winds, and therefore the divergent winds can be neglected (Davis and Emanuel 1991; BY94b). The θ_b fields exhibit mesoscale structures in both cases and the magnitude of the thermal anomaly are similar at the cyclone centers (Fig. 11a and 11d). The intense warm front, with its strong thermal gradients to the east northeast, can be identified in both cyclones. The wind fields show broad synoptic-scale cyclonic circulation around the warm anomalies and anticy-

clonic circulation around the cold thermal anomalies.

In the moist case, the PV anomaly at 800 mb (Fig. 11e) shows the remnants of the latent heat release in the bent-back warm frontal zone. The positive anomaly exhibits mesoscale features and it almost encircles the cyclone center where a cyclonic circulation can be noted. A similar positive anomaly, although not as intense as in the moist case, with associated mesoscale features (Fig. 11b), also appears in the dry cyclone along the frontal regions. The equation for the PV evo-

TABLE 1. Percentage contribution of the three dynamically significant anomalies at different times to dry (moist) cyclogenesis.

Time (day)	θ_B	LPV	UPV
1.0	78.8 (72.0)	11.2 (8.5)	10.0 (19.5)
2.0	71.7 (50.4)	5.0 (36.2)	23.3 (13.4)
3.0	40.5 (12.8)	23.6 (47.2)	35.9 (40.0)
4.0	31.5 (29.5)	30.2 (35.5)	38.3 (35.0)
5.0	28.3 (24.5)	30.4 (33.5)	31.3 (42.0)
6.0	34.5 (22.4)	24.2 (33.8)	41.3 (43.8)
7.0	37.1 (27.7)	20.8 (28.8)	42.1 (43.8)
8.0	41.2 (33.7)	19.2 (26.7)	39.6 (39.6)
9.0	36.7 (31.6)	23.6 (24.6)	39.7 (43.8)
10.0	34.5 (26.9)	26.5 (31.1)	39.0 (42.0)

lution in our hydrostatic p -coordinate model is given by

$$dP/dt = g[\partial(X, \theta)/\partial(y, p) - \partial(\theta, Y)/\partial(x, p) + \partial(u - fy, Q)/\partial(y, p) - \partial(v, Q)/\partial(x, p)], \quad (7)$$

where P is given by (6), and

$$\partial(A, B)/\partial(x, y) = \partial A/\partial x \partial B/\partial y - \partial A/\partial y \partial B/\partial x$$

$$X = v\nabla^2 u, \quad Y = v\nabla^2 v \quad \text{and} \quad Q = d\theta/dt = v\nabla^2 \theta + H.$$

The symbol H represents the surface heat flux in the boundary layer. Therefore, the positive anomaly at 800 mb in the dry cyclone can arise because of internal diffusion of momentum or heat in the frontal region. Taking liberal estimates for various quantities ($v = 0.35 \times 10^5 \text{ m s}^{-2}$, $\Delta y = 0.25 \times 10^5 \text{ m}$, $\Delta u = 10 \text{ m s}^{-1}$, $\Delta\theta/\Delta p = 10 \text{ K}/1000 \text{ mb}$ for a frontal zone) for one of the terms such as $g(v\nabla^2 u/\Delta y)(\partial\theta/\partial p)$, the PV tendency due to momentum diffusion could be as high as 1.5 pvu per day. The PV generation due to latent heat release in our model was about 3.5–4 pvu per day. Therefore, even though there is no PV generation due to latent heat release, the diffusion in the frontal region can generate LPV in the dry cyclone. The diffusive effects operate in the moist model as well. A similar estimate due to horizontal heat diffusion has been derived by Cooper et al. (1992) for a mesoscale frontal region. Keyser and Anthes (1982) showed that in the warm sector, the diabatic term related to vertical heat flux is a major source of positive PV anomaly. The implications of these PV generation due to mixing for equilibration (stabilization) of the baroclinic wave in simple two-dimensional models has been discussed in Nakamura and Held (1989) and Garner et al. (1992).

The 300-mb PV anomaly on day 5 shows large positive values associated with the upper-level trough over the cyclone center (Figs. 11c and 11f). The negative anomaly associated with the ridge is slightly stronger in the moist case. This behavior is attributable to the

warm conveyor belt that carries upward the negative PV produced above the level of maximum condensational heating in the warm frontal zone. The resulting separation of the condensation-created positive LPV from the associated negative UPV is crucial because if positive and negative anomalies are aligned vertically, a cancellation of their effects would occur (Eliassen and Kleinschmidt 1957). Note that the moist cyclone exhibits two positive maxima (Fig. 11f) against a single maximum in the dry case (Fig. 11c). The enhanced southward extrusion of high PV also can be noticed (Fig. 11f). The air motion associated with the 300-mb PV anomaly reveals a well-defined synoptic-scale cyclonic and anticyclonic circulations at 900 mb in both simulations.

4. Conclusions

The primary motivation for this paper has been to further examine the full life cycle of the simulated marine cyclone presented in BY94b. We were also interested in understanding the departure of the moist dynamics from dry baroclinic dynamics from an energetics point of view as well as in terms of "PV thinking." To this end, certain quantities related to energetics are analyzed and the quantitative effect of convection through the life cycle is explored with a PV diagnostics tool recently developed by Davis and Emanuel (1991) and used in BY94b.

The major departure of the moist cyclone from the dry cyclone is its mesoscale features during the early rapid spinup period. These features are presented in detail in BY94b. In particular, the vorticity field has a crescent-shaped structure whose scale is only 200 km and whose maximum value exceeds $10f_0$. The previous life cycle simulations of dry cyclones have indicated that the cold front is stronger than the warm front. We find contrary results for a marine cyclone when the effect of latent heat release is included.

From an energetics point of view, we noticed that the dynamics of the moist cyclone is very similar, but enhanced, in comparison to the dry baroclinic dynamics. The cumulative effect of latent heat release is to contribute up to 50% to the overall eddy kinetic energy growth. The evolution of eddy kinetic energy, energy conversions from eddy APE to eddy KE and from zonal KE to eddy KE, and the domain-averaged eddy heat and momentum fluxes in the moist case closely resemble the dry cyclone. However, it should be noted that there are differences between moist and dry cyclones in the finer details in the spinup period. For instance, the meridional cross section of eddy KE density indicates the trapping of energy near the warm and bent-back warm frontal regions in the moist cyclone. Moreover, the moist cyclone exhibits a larger amplitude in terms of eddy KE, the energy conversion rates, the domain-averaged eddy heat and momentum fluxes, and decay rate.

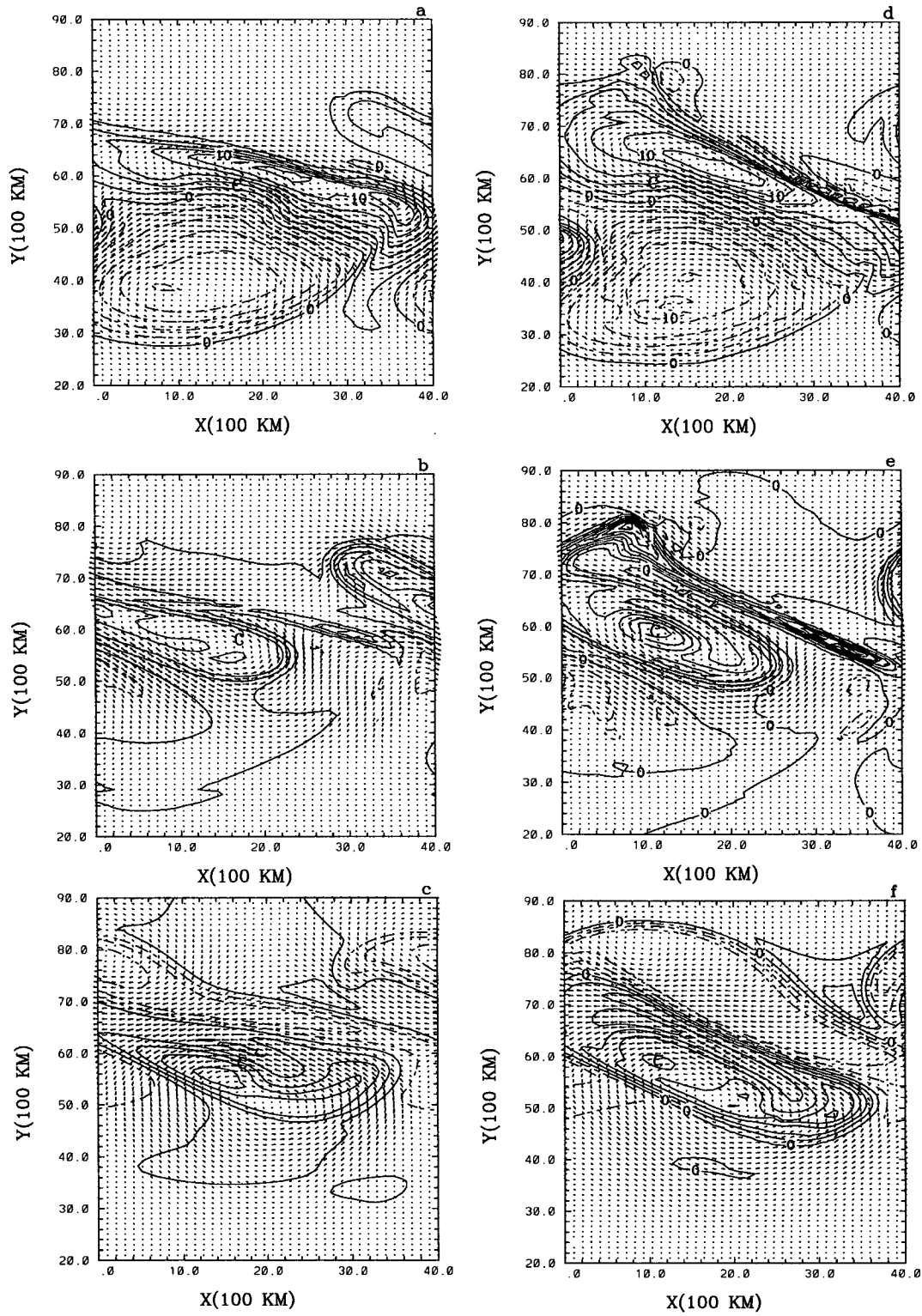


FIG. 11. The results of PV diagnostics for the dry and moist cyclones at 5 days. The surface (1000 mb) θ anomaly every 2 K and the nondivergent wind field at 900 mb associated with this anomaly for the (a) dry and (d) moist cyclone. The PV anomaly at 800 mb and the corresponding wind field at 900 mb for the (b) dry and (e) moist cyclone. The contour interval is 0.2 pvu. Panels (c) and (f) are the same as (b) and (e), but at 300 mb and the contour interval is 1.0 pvu.

The PV diagnostics reveal that the PV anomaly produced by latent heat release contributes up to 50% to the low-level cyclonic circulation. In the dry cyclone also, the low-level PV contributes a substantial percentage to the circulation in the mature stage. However, the origin of this PV anomaly in the dry cyclone is related to diffusion in the frontal region. The cyclolytic effect of convection in inducing the cold advection in the bent-back warm frontal region and thereby reducing the warm anomaly over the cyclone center is in agreement with the earlier result reported in BY94b. The sharp increase of the UPV contribution to surface cyclogenesis in the moist cyclone on day 2 coincides with the decrease of the contribution from surface thermal anomaly. This is consistent with our earlier findings (BY94a, BY94b) that the cold advection in the bent-back warm frontal region leads to enhanced upper-level vorticity advection. The latent heating-induced anti-cyclonic circulation in the ridge region also is partly responsible for the increased vorticity advection. In summary, from a PV perspective, the main difference between the moist and dry cyclone is the production of LPV due to condensation in association with the meso-scale structures in the warm frontal zone and its effects on the moist cyclone during the early rapid spinup stage.

We caution about the direct application of our results to the real atmosphere. We have used an idealized initial condition and a very simple formulation for the latent heat release. We have omitted detailed cloud microphysics, convective parameterization, surface friction, topography, radiation, etc. The results may be, therefore, more applicable to moderately intense marine cyclones than to extremely intense storms like QEII (Gyakum 1983a, 1983b).

We should point out that the presence of vertical walls at the north and south boundaries imposes a severe constraint on the duration of the idealized life cycle experiments. The use of spherical geometry is also important for a complete understanding of the moist life cycle (Whitaker and Snyder 1993), even though the evolution of the cyclones was very similar on the f - (BY94b) and beta-planes during the time of the rapid spinup, indicating that the effect of earth's sphericity may not be significant during this period. However, it is recognized that the nonlinear barotropic governor can be very different on the sphere (Nakamura 1993), and the nonlinear evolution and the final equilibration of the baroclinic waves are very sensitive to the different asymmetries (ageostrophy, beta, sphericity, etc.) introduced into the model (James 1987; Nakamura 1993). Also, the wave breaking and the rapid decay of the cyclones found in our beta-plane channel model simulations did not occur in a study of baroclinic waves on the sphere by Thorncroft et al. (1993), who found very little barotropic decay in a case labeled LC2, where the trough intensifies to form a steady vortex on the cyclonic side. They argued that when the eddies

intensify on the cyclonic side on a sphere, Rossby wave radiation to the subtropics does not take place. But as was shown in our Cartesian plane simulations, the eddies can decay locally on the cyclonic side without radiation to the south. This occurs also in additional dry experiments with wider channels where the eddies still undergo rapid barotropic decay on the cyclonic side. The observation in section 3b that the horizontal eddy momentum fluxes were equatorward and the wave breaking was cyclonic (as opposed to the typical anti-cyclonic wave breaking on the sphere) has led us to a study of the relevance of the structure of eddy momentum fluxes to the type of wave breaking and a thorough investigation of the effect of spherical geometry on baroclinic decay process. We will report on these results in a future paper.

Acknowledgments. This research was supported by the U.S. Office of Naval Research Grant N00014-87-J-1171, the Atmospheric Environment Service, and the Natural Sciences and Engineering Research Council of Canada. The authors thank Dr. S. T. Garner of GFDL for helpful comments on an earlier version of the paper. The authors also thank the anonymous reviewers for their comments.

REFERENCES

- Balasubramanian, G., and M. K. Yau, 1994a: Baroclinic instability in a two layer model with parameterized slantwise convection. *J. Atmos. Sci.*, **51**, 971–990.
- , and —, 1994b: The effects of convection on a simulated cyclone. *J. Atmos. Sci.*, **51**, 2397–2417.
- , and —, 1995: Explosive marine cyclogenesis in a three-layer model with a representation of slantwise convection: A sensitivity study. *J. Atmos. Sci.*, **52**, 533–550.
- Bennetts, D. A., and J. C. Sharp, 1982: The relevance of conditional symmetric instability to the prediction of mesoscale rainbands. *Quart. J. Roy. Meteor. Soc.*, **108**, 595–602.
- Cooper, I. M., A. J. Thorpe, and C. H. Bishop, 1992: The role of diffusive effects on potential vorticity in fronts. *Quart. J. Roy. Meteor. Soc.*, **118**, 629–647.
- Danard, M. B., 1964: On the influence of released latent heat on cyclone development. *J. Appl. Meteor.*, **3**, 27–37.
- Davis, C. A., and K. A. Emanuel, 1991: Potential vorticity diagnostics of cyclogenesis. *Mon. Wea. Rev.*, **119**, 1929–1953.
- Edmon, H. J., B. J. Hoskins, and M. E. McIntyre, 1980: Eliassen–Palm cross sections for the troposphere. *J. Atmos. Sci.*, **37**, 2600–2616.
- Eliassen, A., and E. Kleinschmidt, 1957: *Dynamic Meteorology*. Vol. 48, *Handbuch der Physik*, Springer Verlag, 154 pp.
- Emanuel, K. A., 1988: Observational evidence of slantwise convective adjustment. *Mon. Wea. Rev.*, **116**, 1805–1816.
- , M. Fantini, and A. J. Thorpe, 1987: Baroclinic instability in an environment of small stability to slantwise moist convection. Part I: Two-dimensional models. *J. Atmos. Sci.*, **44**, 1559–1573.
- Fantini, M., 1990: The effect of heat and moisture fluxes from the ocean on the development of baroclinic waves. *J. Atmos. Sci.*, **47**, 840–855.
- , 1993: A numerical study of two-dimensional moist baroclinic instability. *J. Atmos. Sci.*, **50**, 1199–1210.
- Gall, R. L., 1976: The effects of released latent heat in growing baroclinic waves. *J. Atmos. Sci.*, **33**, 1686–1701.
- Garner, S. T., N. Nakamura, and I. M. Held, 1992: Nonlinear equilibration of two-dimensional Eady waves: A new perspective. *J. Atmos. Sci.*, **49**, 1984–1996.

- Gutowski, W. J., L. E. Branscome, and D. S. Stewart, 1992: Life cycles of moist baroclinic eddies. *J. Atmos. Sci.*, **49**, 306–319.
- Gyakum, J. R., 1983a: On the evolution of QE II storm. Part I: Synoptic aspects. *Mon. Wea. Rev.*, **111**, 1137–1155.
- , 1983b: On the evolution of QE II storm. Part II: Dynamic and thermodynamic structure. *Mon. Wea. Rev.*, **111**, 1156–1173.
- Hedley, M., and M. K. Yau, 1991: Anelastic modeling of explosive cyclogenesis. *J. Atmos. Sci.*, **48**, 711–727.
- Holton, J. R., 1992: *An Introduction to Dynamic Meteorology*. 3d ed., Academic Press, 511 pp.
- James, I. N., 1987: Suppression of baroclinic instability in horizontally sheared flows. *J. Atmos. Sci.*, **44**, 3710–3720.
- Joly, A., and A. J. Thorpe, 1989: Warm and occluded fronts in two-dimensional moist baroclinic instability. *Quart. J. Roy. Meteor. Soc.*, **115**, 513–534.
- Keyser, D., and R. A. Anthes, 1982: The influence of planetary boundary-layer physics on frontal structure in the Hoskins–Bretherton horizontal shear model. *J. Atmos. Sci.*, **42**, 1783–1802.
- Kuo, Y.-H., and R. J. Reed, 1988: Numerical simulation of an explosively deepening cyclone in the eastern Pacific. *Mon. Wea. Rev.*, **116**, 2081–2105.
- , M. A. Shapiro, and E. G. Donall, 1991a: The interaction of baroclinic and diabatic processes in a numerical simulation of rapidly intensifying extratropical marine cyclone. *Mon. Wea. Rev.*, **119**, 368–384.
- , R. J. Reed, and S. Low-Nam, 1991b: Effects of surface energy fluxes during the early development and rapid intensification stages of winter cyclones in the western Atlantic. *Mon. Wea. Rev.*, **119**, 457–476.
- Liou, C. S., and R. L. Elsberry, 1987: Heat budgets analyses and forecasts of an explosively deepening maritime cyclone. *Mon. Wea. Rev.*, **115**, 1809–1824.
- Lorenz, E. N., 1955: Available potential energy and the maintenance of the general circulation. *Tellus*, **7**, 157–167.
- Manabe, S., 1956: On the contribution of heat released by condensation to the change in pressure pattern. *J. Meteor. Soc. Japan*, **34**, 12–24.
- Mudrick, S., 1974: A numerical study of frontogenesis. *J. Atmos. Sci.*, **31**, 869–892.
- Nakamura, N., 1993: Momentum flux, flow symmetry, and the nonlinear barotropic governor. *J. Atmos. Sci.*, **50**, 2159–2179.
- , and I. M. Held, 1989: Nonlinear equilibration of two-dimensional Eady waves. *J. Atmos. Sci.*, **46**, 3055–3064.
- Paused, J. P., and A. H. Oort, 1984: Physics of climate. *Rev. Modern Phys.*, **56**, 367–429.
- Polavarapu, S. M., and W. R. Peltier, 1990: The structure and nonlinear evolution of synoptic scale cyclones: Life cycle simulations with a cloud-scale model. *J. Atmos. Sci.*, **47**, 2645–2672.
- Reuter, G. W., and M. K. Yau, 1990: Observation of slantwise convective instability in winter cyclones. *Mon. Wea. Rev.*, **118**, 447–458.
- , and ———, 1993: Assessment of slantwise convection in ERICA cyclones. *Mon. Wea. Rev.*, **121**, 375–386.
- Rotunno, R., W. C. Skamarock, and C. Snyder, 1994: An analysis of frontogenesis in numerical simulation of baroclinic waves. *J. Atmos. Sci.*, **51**, 3373–3398.
- Sanders, F., and L. F. Bosart, 1985: Mesoscale structure in the megaloopolitan snowstorm of 11–12 February 1983. Part I: Frontogenetical forcing and symmetric instability. *J. Atmos. Sci.*, **42**, 1050–1061.
- Shapiro, M. A., and D. Keyser, 1990: Fronts, jet streams and the tropopause. *Extratropical Cyclones, Palmén Memorial Volume*, C. W. Newton and E. O. Holopainen, Eds., Amer. Meteor. Soc., 262 pp.
- Simmons, A. J., and B. J. Hoskins, 1978: The life cycles of some nonlinear baroclinic waves. *J. Atmos. Sci.*, **35**, 414–432.
- , and ———, 1980: Barotropic influences on the growth and decay of nonlinear baroclinic waves. *J. Atmos. Sci.*, **37**, 1679–1684.
- Smagorinsky, J., 1956: On the numerical integration of the primitive equations of motion for baroclinic flows in a closed region. *Mon. Wea. Rev.*, **86**, 457–466.
- Snyder, C., and R. S. Lindzen, 1991: Quasi-geostrophic wave-CISK in unbounded baroclinic shear. *J. Atmos. Sci.*, **48**, 76–86.
- Takayabu, I., 1986: Roles of the horizontal advection on the formation of surface fronts and on the occlusion of a cyclone developing in a baroclinic westerly jet. *J. Meteor. Soc. Japan*, **64**, 329–345.
- Thorncroft, C. D., B. J. Hoskins, and M. E. McIntyre, 1993: Two paradigms of baroclinic wave life-cycle behavior. *Quart. J. Roy. Meteor. Soc.*, **119**, 17–55.
- Thorpe, A. J., and K. A. Emanuel, 1985: Frontogenesis in the presence of small stability to slantwise convection. *J. Atmos. Sci.*, **42**, 1809–1824.
- Tracton, M. S., 1973: The role of cumulus convection in the development of extratropical cyclone. *Mon. Wea. Rev.*, **101**, 573–593.
- Wang, B., and A. Barcion, 1986: Moist stability of a baroclinic zonal flow with conditionally unstable stratification. *J. Atmos. Sci.*, **43**, 705–719.
- Whitaker, J. S., and C. Snyder, 1993: The effects of spherical geometry on the evolution of baroclinic waves. *J. Atmos. Sci.*, **50**, 597–612.
- , and C. A. Davis, 1994: Cyclogenesis in a saturated environment. *J. Atmos. Sci.*, **51**, 889–907.
- Xu, Q., 1988: Baroclinic waves and frontogenesis with embedded regions of small moist symmetric stability. *Quart. J. Roy. Meteor. Soc.*, **114**, 1221–1251.
- , 1990: Cold and warm frontal circulations in an idealized moist semigeostrophic baroclinic wave. *J. Atmos. Sci.*, **47**, 2337–2352.